Lawrence Berkeley National Laboratory

Title

Ex-situ metrology and data processing techniques developed at the ALS for optimization of beamline performance of bendable x-ray mirrors

Permalink

Authors

Yashchuk, Valeriy V
Lacey, Ian
McKinney, Wayne R

Peer reviewed

Ex situ metrology and data processing techniques developed at the ALS for optimization of beamline performance of bendable x-ray mirrors

Valeriy V. Yashchuk,* Ian Lacey, and Wayne R. McKinney

Advanced Light Source Berkeley, Lawrence Berkeley National Laboratory, California 94720, USA

ABSTRACT

We discuss experimental, analytical, and numerical methods recently developed at the Advanced Light Source (ALS) X-Ray Optics Laboratory (XROL) for calibration and precision shaping of bendable x-ray mirrors. The methods are based on ex situ measurements with the mirrors using surface slope profilers available at the ALS XROL. The first realization of methods and dedicated software has allowed the optimization of the beamline performance of bendable mirrors by adjustment of the mirror shape to minimize the root-mean-square variation of residual (after subtraction of the ideal desired shape) slope deviations from ideal (specified) surface figure. Here, we further develop the methods that in application to elliptically bent mirrors adapt as a figure of merit the minimum of the rms size of the focused beam. The efficacy of the developed methods is demonstrated with examples of optimal tuning of an elliptically bendable cylindrical mirror designed for the ALS beamline 10.3.2.

Keywords: X-ray mirrors, bendable mirrors, adaptive optics, ex situ metrology, surface slope profilometry, long trace profiler, synchrotron radiation, X-rays

1. INTRODUCTION

For simultaneous focusing of x-ray beams in the orthogonal tangential and sagittal directions, two elliptically cylindrical reflecting mirrors, a Kirkpatrick-Baez (KB) pair are usually used.[1] In x-ray microscopes, Wolter optical systems,[2,3] consisting of a hyperbolic mirror followed by an elliptical mirror, are often used to make a compact system. Because fabrication of aspherical surfaces is complicated, the cost of directly fabricated tangential elliptical and hyperbolic cylinders is often prohibitive. Moreover, pre-shaped optics cannot be easily readjusted for use in multiple, different experimental arrangements, e.g. at different focal distances.[4] This is in contrast to flat optics that are simpler to manufacture and easier to measure by conventional metrology tools, such as commercial large aperture Fizeau interferometers. In bendable x-ray optics, the tangential figure of a flat substrate is changed by placing torques (couples) at each end of the substrate. Depending on the applied couples and the variation of the sagittal width of the substrate, one can tune the shape of a bendable mirror close to a desired profile, for example, tangential cylinder, parabola, or ellipse.[5,6]

High performance of a bendable mirror at the beamline relies on the quality of design and the accuracy of fabrication of the mirror substrate and benders, as well as on the capability of ex situ (at optics lab) and in situ (at beamline) metrology to optimally tune the mirror, getting the surface profile as close to the desired shape as possible, compensating for the design and fabrication errors.

In this paper, we provide a systematic description of experimental, analytical, and numerical methods[7-18] recently developed at the Advanced Light Source (ALS) X-Ray Optics Laboratory (XROL)[19,20] for optimization of beamline performance of bendable x-ray optics used for focusing of beams of soft and hard x-rays at the ALS. We concentrate the discussion on the methods that are based on geometrical optics and optical surface slope metrology available at the ALS XROL with three state-of-the-art surface slope profilers, the Long Trace Profiler LTP-II,[21,22] Developmental LTP, DLTP,[23,24] and Optical Surface Measuring System, OSMS.[25,26] Methods of in situ optimization of bendable optics developed at the ALS XROL[27-29] are not considered here.

The paper is organized as follows. First, we review the nature of the requirements for bending and approaches to the substrate design (Sec 2). Next (Sec. 3), we provide mathematical foundations of the method of characteristic functions[7,8,30] in application for ex situ optimal tuning of bendable optics. In the original formulation of the method, the figure of merit of the tuning is the minimum of the root-mean-square (rms) deviation of the bent profile in the slope

*vvyashchuk@lbl.gov;   phone 1 510 495-2592;   fax 1 510 486-7696

domain from the desired one determined by the parameters of beamline usage (the conjugate parameters) of a mirror. Here, we extend the consideration to the case of the weighted rms slope deviations that allows accounting for non-uniform distribution of the x-ray beamline intensity. In Sec. 4, we derive the analytical expressions describing the tangential surface slope and height profile of an ideal elliptically cylindrical mirror as functions of the mirror conjugate parameters. Using the derived analytical expressions, we further develop the method in application to elliptically bent mirrors to adapt as a figure of merit the minimum of the rms size of the focused beam (Sec. 5). Realization of the developed analytical methods in dedicated software and an application of the software is discussed and demonstrated in Sec. 6. The software allows optimization of beamline performance of the mirror by finest adjustment of the mirror benders to best match the ideal (specified) surface figure, with accounting for beamline application geometry of the mirror and for the no-uniform distribution of intensity of the incident x-ray beam. The efficacy of the developed methods is demonstrated with examples of optimal tuning of an elliptically bendable cylindrical mirror designed for the ALS beamline 10.3.2.

2. BENDING WITH TWO BENDING MOMENTS APPLIED TO THE ENDS OF A PLANE SUBSTRATE

The basic theory of bendable mirrors has been well described in the literature.[5,6] The bending of a thin mirror substrate is described by the Bernoulli-Euler equation:[31]

$$E\,I(x)\frac{d^2 y}{dx^2} = \frac{C_1 + C_2}{2} + \frac{C_1 - C_2}{L}\,x\,,$$

(1)

where E is the elastic modulus, $I(x)$ is the moment of inertia as a function of the tangential distance along the mirror, x (we assume that $x = 0$ at the mirror center), C_1 and C_2 are the bending moments (couples) applied to the ends of the mirror substrate, and L is the mirror length (Fig. 1).
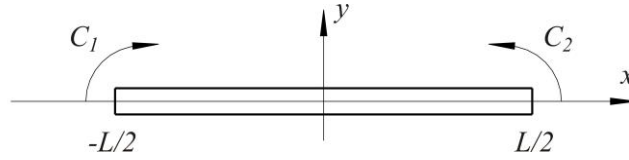

Figure 1. Bending of a plane mirror substrate with length L with two couples C_1 and C_2 applied to the ends of the substrate. C_2 is typically the downstream adjustment. Arrows define positive couples.

For a substrate with rectangular cross-section, the moment of inertia depends on the local sagittal width $w(x)$ and thickness $t(x)$:[31]

$$I(x) = w(x)\,t^3(x)/12\,.$$

(2)

According to Eqs. (1) and (2), a substrate with uniform cross-section, $w(x) = w_0$ and $t(x) = t_0$, can be bent only to the shape in the height domain described by a third order polynomial. This case includes bending to a parabolic (cylindrical) profile at $C_1 = C_2$. Bending to more sophisticated shapes (for example, elliptical or hyperbolic), which are not described by third order polynomials, requires substrates with a non-uniform cross-section.[5,6] From the fabrication point of view, profiling of the sagittal width at constant thickness, $I(x) = w(x)\,t_0^3/12$, is more practical.

An analytical expression for the optimal sagittal width as a function of x can be easily derived from Eq. (1) for the known desired mirror profile $y(x)$ and selected couples C_1 and C_2:[9,16]

$$w(x) = \frac{12}{E\,t_0^3}\left(\frac{C_1 + C_2}{2} + \frac{C_1 - C_2}{L}\,x\right)\Big/\frac{d^2 y}{dx^2}\,.$$

(3)

In Sec. 4, we derive the analytical expressions describing the tangential height profile and its first and second derivatives of an ideal elliptically cylindrical mirror as functions of the mirror conjugate parameters. Substituting the derived expression for the second derivative in Eq. (3), one can calculate the sagittal width variation optimal for the elliptically bent mirrors.

3. METHOD OF CHARACTERISTIC FUNCTIONS

Usually, the design of the mirror bending mechanism does not allow a direct high-precision measurement of the bending couples and setting them to values pre-calculated in the course of the mirror design. But even were such a measurement possible, such settings are generally not accurate enough due to fabrication tolerances. In this section, we provide mathematical foundations of the method of characteristic functions[30] for optimal tuning of bendable optics experimentally by using ex situ surface slope metrology.[7,8] The idea of the experimental estimation of the bender characteristic functions was suggested in Ref.[30] in application to fine adjustment of bendable KB mirrors at the beamline. Unfortunately, the mathematical description in Ref.[30] contains an omission (perhaps inadvertent, see also discussion in Sec. 3.2) that makes straightforward usage of the described optimization algorithm impractical.

3.1 Bender's characteristic functions

The idea of the method of characteristic functions consists in application linear regression analysis to the system of two benders, experimentally calibrated in a series of dedicated measurements. It is possible due to the linearity of Eq. (1) with respect to the couples C_1 and C_2. Indeed, with straightforward transformations, Eq. (1) can be rewritten in the terms of surface slope variation $\alpha(x,\hat{C}) \equiv \alpha(x,C_0,C_1,C_2)$, corresponding to the particular values of the bending couples:[7,8]

$$\alpha(x,\hat{C}) \approx \tan\left[\alpha(x,\hat{C})\right] \equiv \frac{dy}{dx} = C_0 + C_1 f_1(x) + C_2 f_2(x), \tag{4}$$

where C_0 is a constant of integration that is an overall tilt of the mirror, and $f_1(x)$ and $f_2(x)$ are the bender's characteristic functions defined as

$$f_1(x) = \int \left(\frac{1}{2} - \frac{1}{L} x\right) \frac{dx}{EI(x)} \quad \text{and} \quad f_2(x) = \int \left(\frac{1}{2} + \frac{1}{L} x\right) \frac{dx}{EI(x)}, \tag{5}$$

According to Eq. (4), the slope trace of a bendable mirror is a linear combination of two functions, $f_1(x)$ and $f_2(x)$ characteristic for the particular mirror design. These functions can be approximately determined from three surface slope measurements over the set of discrete positions x_i, two of which are repeated at the known changes of the bending couples, δC_1 and δC_2:

$$\alpha_1(x_i,C_1,C_2), \quad \alpha_2(x_i,C_1 + \delta C_1,C_2), \quad \text{and} \quad \alpha_3(x_i,C_1,C_2 + \delta C_2). \tag{6}$$

Here, C_1 and C_2 are the adjustments of the bendable mirror in whatever units are convenient for the designed bender mechanism and $i = 1,...,n$, where n is the total number of points in the measured traces.

Neglecting the measurement error, the approximated characteristic functions experimentally measured in the discrete positions x_i are

$$f_1^*(x_i) = \frac{\alpha_2(x_i,C_1 + \delta C_1,C_2) - \alpha_1(x_i,C_1,C_2)}{\delta C_1}, \quad \text{and} \tag{7a}$$

$$f_2^*(x_i) = \frac{\alpha_3(x_i,C_1,C_2 + \delta C_2) - \alpha_1(x_i,C_1,C_2)}{\delta C_2}. \tag{7b}$$

With the asterisk, we separate the estimate from the true value of the function.

3.2 Linear regression analysis in application for ex situ tuning of bendable mirrors

With the experimentally determined characteristic functions $f_1^*(x_i)$ and $f_2^*(x_i)$ given with Eqs. (7a,b), we approximate (best fit) the deviation $\Delta(x_i)$ of the measured surface slope distribution $\alpha^M(x_i)$ from the desired (ideal) one $\alpha^0(x_i)$, calculated for the same set of positions:

$$\Delta(x_i) \equiv \alpha^0(x_i) - \alpha^M(x_i) = \xi_0 + \xi_1 f_1^*(x_i) + \xi_2 f_2^*(x_i) + \varepsilon_i \,, \tag{8}$$

where ε_i is the approximation error that generally also includes the fabrication error of the substrate surface, the measurement error, and the error of the estimation of the characteristic functions. Throughout the present paper, we assume that the measurement and the estimation errors are negligible compared to the surface slope error due to the fabrication process, and as such, inherent to the mirror surface. However, this assumption is not critical for the successful application of the methods under discussion.

The conventional approach to finding the adjustment parameters in Eq. (8) is to fit the slope error with the characteristic functions by minimizing the sum of the squared approximation errors, the method of least squares. In a case such as ours, when the fitting function can be expanded into a linear (over the parameters ξ_0, ξ_1, and ξ_2) combination of some known (experimentally determined) functions, the method of linear regression analysis provides a way for direct calculation of the parameters.[32,33] For tuning a bendable mirror, the couple's adjustments ξ_1 and ξ_2 determined together with ξ_0 in the course of the fitting have to be added to the settings C_1^M and C_2^M used in the measurement of the slope distribution $\alpha^M(x_i)$.

We provide below a condensed narration of the method of linear regression analysis in application for tuning of bendable mirrors using notations of the book,[32] chosen by the authors as a preferred reference due to its compact format of comprehensive contents. Unfortunately, the book[32] has limited availability. A condensed version of the related material can be found in Ref.[33] A more detailed discussion of linear regression analysis with extensive proofs of formulae used below can be found in more fundamental books (see, for example, Refs.[34-36]).

Let us express the approximation error by rewriting (8) as

$$\varepsilon_i = \Delta(x_i) - \xi_0 - \xi_1 f_1^*(x_i) - \xi_2 f_2^*(x_i) \,, \tag{9}$$

Assuming that dispersion functions of the ε_i are identical with equal variance σ^2, the best-fitting regression function (8) corresponds to the minimum of the sum of squared approximation errors over n measured points:

$$S = \sum_{i=1}^{n} \varepsilon_i^2 = \sum_{i=1}^{n} \left(\Delta(x_i) - \xi_0 - \xi_1 f_1^*(x_i) - \xi_2 f_2^*(x_i) \right)^2 \,, \tag{10}$$

while the parameters θ_ρ are varied

$$\frac{\partial S}{\partial \xi_0} = -2 \sum_{i=1}^{n} \left(\Delta(x_i) - \xi_0 - \xi_1 f_1^*(x_i) - \xi_2 f_2^*(x_i) \right) = 0 \,, \tag{11a}$$

$$\frac{\partial S}{\partial \xi_1} = -2 \sum_{i=1}^{n} f_1^*(x_i) \left(\Delta(x_i) - \xi_0 - \xi_1 f_1^*(x_i) - \xi_2 f_2^*(x_i) \right) = 0 \,, \tag{11b}$$

$$\frac{\partial S}{\partial \xi_2} = -2 \sum_{i=1}^{n} f_2^*(x_i) \left(\Delta(x_i) - \xi_0 - \xi_1 f_1^*(x_i) - \xi_2 f_2^*(x_i) \right) = 0 \,. \tag{11c}$$

The system of equations (11) can be transformed to the *normal* equations:

$$n\xi_0 + \xi_1 \sum_{i=1}^{n} f_1^*(x_i) + \xi_2 \sum_{i=1}^{n} f_2^*(x_i) = \sum_{i=1}^{n} \Delta(x_i) \,, \tag{12a}$$

$$\xi_0 \sum_{i=1}^{n} f_1^*(x_i) + \xi_1 \sum_{i=1}^{n} f_1^*(x_i) f_1^*(x_i) + \xi_2 \sum_{i=1}^{n} f_1^*(x_i) f_2^*(x_i) = \sum_{i=1}^{n} f_1^*(x_i)\Delta(x_i)\,, \tag{12b}$$

$$\xi_0 \sum_{i=1}^{n} f_2^*(x_i) + \xi_1 \sum_{i=1}^{n} f_2^*(x_i) f_1^*(x_i) + \xi_2 \sum_{i=1}^{n} f_2^*(x_i) f_2^*(x_i) = \sum_{i=1}^{n} f_2^*(x_i)\Delta(x_i)\,. \tag{12c}$$

The solution of the system (12) can be simplified if one uses matrix approach. First, introduce an $n \times 3$ matrix termed the *regression* matrix,

$$\hat{A} = \begin{bmatrix} 1 & f_1^*(x_1) & f_2^*(x_1) \\ 1 & f_1^*(x_2) & f_2^*(x_2) \\ \vdots & \vdots & \vdots \\ 1 & f_1^*(x_m) & f_2^*(x_m) \end{bmatrix}. \tag{13}$$

and a 1×3 vector of parameters with the prime denoting a transposed matrix:

$$\hat{\xi}' = \left(\xi_0, \xi_1, \xi_2 \right). \tag{14}$$

In matrix form, equations (9) and (10) can be rewritten as

$$\hat{\varepsilon} = \hat{\Delta} - \hat{A}\hat{\xi}\,, \tag{15}$$

$$S = \hat{\varepsilon}'\hat{\varepsilon} = (\hat{\Delta} - \hat{A}\hat{\xi})'(\hat{\Delta} - \hat{A}\hat{\xi}) = \hat{\Delta}'\hat{\Delta} - 2\hat{\xi}'\hat{A}'\hat{\Delta} + \hat{\xi}'\hat{A}'\hat{A}\hat{\xi}\,, \tag{16}$$

where $\hat{\Delta}$ and $\hat{\varepsilon}$ are $1 \times n$ vectors with the elements $\Delta_i = \Delta(x_i)$ and ε_i, respectively.

By differentiating Eq. (16), one can get the system of equations equivalent to Eqs. (11) and (12)

$$-2\hat{A}'\hat{\Delta} + 2\hat{A}'\hat{A}\,\hat{\xi} = 0\,, \tag{17}$$

$$(\hat{A}'\hat{A})\,\hat{\xi} = \hat{A}'\hat{\Delta}\,. \tag{18}$$

If the matrix $\hat{A}'\hat{A}$ is a full rank matrix, the solution of the system (18) is

$$\hat{\xi}^* = (\hat{A}'\hat{A})^{-1}\hat{A}'\hat{\Delta}\,. \tag{19}$$

A singularity can appear in the case when the estimation is performed for an excessive number of parameters. In other words, excessiveness is observed if any lines of matrix $\hat{A}$ are linearly dependent. This is certainly not true for the case of the characteristic functions of two benders at the opposite ends of a bendable mirror; and regression analysis in application for optimal tuning bendable mirror appears to be very effective.[14-17]

It can be shown that the estimate (19) gives an unbiased estimate of the parameters $\hat{\xi}$, meaning the expectation of $\hat{\xi}^*$ is $\hat{\xi}$. Moreover, the estimate $\hat{\xi}^*$ is the most accurate among all possible unbiased estimates. In the case of independent slope measurements with equal variance σ^2, the matrix of errors $\hat{D}$ for the slope deviations is

$$\hat{D}(\hat{\Delta}) = \sigma^2 \, \hat{I}, \tag{20}$$

where $\hat{I}$ is the $n \times n$ unit matrix. Then, the dispersions for adjustment parameters $\hat{\xi}^*$ predicted by the linear regression analysis can be found with a simple relation;[32,33]

$$D(\hat{\xi}^*) = \left((\hat{A}' \hat{A})^{-1} \hat{A}' \right) D\hat{\Delta} \left((\hat{A}' \hat{A})^{-1} \hat{A}' \right)' = \sigma^2 \, (\hat{A}' \hat{A})^{-1}. \tag{21}$$

If the value of σ^2 is unknown, its unbiased estimate σ_*^2 can be found from the sum of squares of the differences (9) between the extrapolating function and the slope deviations Δ_i and the difference between the number of observations n and the number of parameters 3:[32]

$$R = S_{\min} = (\hat{\Delta} - \hat{A}\hat{\xi}^*)'(\hat{\Delta} - \hat{A}\hat{\xi}^*) = \hat{\Delta}'\hat{\Delta} - \hat{\Delta}'\hat{A}\hat{\xi}^*, \tag{22}$$

$$\sigma_*^2 = \frac{R}{n - 3 - 1}. \tag{23}$$

Note that if we leave out the constant term ξ_0, our consideration above is mathematically exactly that, which has been rather briefly outlined in the literature.[30] The constant term omitted in Ref.[30] is an imperative for accurate application of the method. However, the most important difference between the considerations in Refs.[7,8] and those here from those in Ref.[30] is that the linear regression analysis method is grounded and applied for precision tuning of bendable mirrors before installation in the beamline and solely based on surface slope data measured ex situ, in the lab.

From the practical point of view, the application of the linear regression analysis for tuning a bendable mirror requires just a few ex situ surface slope measurements. Three measurements with the benders' settings adjusted according to prescription (6) are needed to build the bender's characteristic functions (7). One of the three measurements (the latest one is more preferable for suppressing the spurious effect due to a backlash possible in the bending mechanism) can be used in the regression analysis as the measured slope distribution $\alpha^M(x_i)$ in Eq. (8). After the predicted adjustments ξ_1^* and ξ_2^* are applied to the benders, one more measurement should be performed to verify the result of the tuning. This last measurement can be used in an additional regression analysis in order to understand if the new predicted adjustments are within the confidence interval for the parameters estimated based on Eqs. (21) – (23). If the second prediction provides statistically significant values of the adjustments (for example, due to a non-ideality of the design and/or fabrication of the bendable mirror), an additional tuning should be made. According to our experience, a bendable mirror appropriately designed and fabricated requires maximum 2-3 tuning iterations that means, requiring only 5-6 slope trace measurements.

3.3 Accounting for x-ray beam intensity distribution along the mirror with weighting matrix

So far, we have assumed that all values of the residual slope error ε_i have the same statistical weight [compare with (20)]. From the point of view beamline application of the mirror, this assumption corresponds to a uniform distribution along the mirror of the reflected x-ray beam intensity, when each surface sub-area defined with index i is equally important for beamline performance of the mirror.

If the assumption about uniform statistical weight of ε_i is not valid (see also discussion in Sec. 5), one can easily generalize the consideration in Sec. 3.2 by assuming the dispersion of ε_i to be weighted with a parameter ω_i, so that

$$\hat{D}(\varepsilon_i) = \sigma^2 \, \hat{W}, \quad D(\varepsilon_i) = \sigma^2 / \omega_i, \tag{24}$$

where $\hat{W}$ is the weighting matrix. This requires minimization of the value of the weighted squared approximation errors [compare with (10)]:

$$S = \sum_{i=1}^{n} \omega_i \, \varepsilon_i^2 . \tag{25}$$

Accordingly, the system of normal equations (12) will look like (assuming $\sum \omega_i = n$; however, we should note that the common normalization of the weighting parameters does not affect the regression result for the values of the predicted adjustments θ_1^* and θ_2^*)

$$n\xi_0 + \xi_1 \sum_{i=1}^{n} \omega_i f_1^*(x_i) + \xi_2 \sum_{i=1}^{n} \omega_i f_2^*(x_i) = \sum_{i=1}^{n} \omega_i \Delta(x_i) , \tag{26a}$$

$$\xi_0 \sum_{i=1}^{n} \omega_i f_1^*(x_i) + \xi_1 \sum_{i=1}^{n} \omega_i f_1^*(x_i) f_1^*(x_i) + \xi_2 \sum_{i=1}^{n} \omega_i f_1^*(x_i) f_2^*(x_i) = \sum_{i=1}^{n} \omega_i f_1^*(x_i) \Delta(x_i) , \tag{26b}$$

$$\xi_0 \sum_{i=1}^{n} \omega_i f_2^*(x_i) + \xi_1 \sum_{i=1}^{n} \omega_i f_2^*(x_i) f_1^*(x_i) + \xi_2 \sum_{i=1}^{n} \omega_i f_2^*(x_i) f_2^*(x_i) = \sum_{i=1}^{n} \omega_i f_2^*(x_i) \Delta(x_i) . \tag{26c}$$

In order to write the system of equation (26) in matrix form, we construct a diagonal matrix

$$\hat{V} = \begin{bmatrix} \left(\sqrt{\omega_1} \right)^{-1} & 0 & 0\ldots & 0 \\ 0 & \left(\sqrt{\omega_2} \right)^{-1} & 0\ldots & 0 \\ \vdots & \vdots & \vdots & \vdots \\ 0 & 0 & 0\ldots & \left(\sqrt{\omega_n} \right)^{-1} \end{bmatrix} , \tag{27}$$

which relates to the weighting matrix $\hat{W}$ via equation

$$\hat{W} = \hat{V} \hat{V}'; \quad \hat{V} = \hat{V}' . \tag{28}$$

We construct also the 'weighted' *regression* matrix [compare with (13)] and 'weighted' matrix of slope deviations

$$\tilde{A} = \hat{V}^{-1} \hat{A} , \tag{29}$$

$$\tilde{\Delta} = \hat{V}^{-1} \hat{\Delta} . \tag{30}$$

Using these notations, the system (26) can be presented in matrix form analogous to (16)

$$S = \tilde{\varepsilon}' \tilde{\varepsilon} = (\tilde{\Delta} - \tilde{A} \hat{\xi})' (\tilde{\Delta} - \tilde{A} \hat{\xi}) = \tilde{\Delta}' \tilde{\Delta} - 2 \hat{\xi}' \tilde{A}' \tilde{\Delta} + \hat{\xi}' \tilde{A}' \tilde{A} \hat{\xi}. \tag{31}$$

And therefore, the equations for finding parameters $\hat{\xi}^*$ will look similar to (19), as well as the equations for the dispersions of the parameters $\hat{\xi}$ will look similar to (21):

$$\hat{\xi}^* = (\tilde{A}' \tilde{A})^{-1} \tilde{A}' \tilde{\Delta} = (\hat{A}' \hat{W}^{-1} \hat{A})^{-1} \hat{A}' \hat{W}^{-1} \hat{\Delta} , \tag{32}$$

$$D(\hat{\xi}^*) = \sigma^2 (\tilde{A}' \tilde{A})^{-1} = \sigma^2 (\hat{A}' \hat{W}^{-1} \hat{A})^{-1} . \tag{33}$$

Finally, one can modify the equations (22) and (23) to get an unbiased estimate σ_*^2 for the 'weighted' slope deviations:

$$\sigma_*^2 = \frac{R}{n-3-1} = \frac{(\hat{\Delta} - \hat{A}\hat{\xi}^*)' \hat{W}^{-1}(\hat{\Delta} - \hat{A}\hat{\xi}^*)}{n-4} . \tag{34}$$

In order to construct the weighting matrix reliably describing the beam intensity distribution and perform the thorough optimization of beamline performance of a bendable mirror, one has to account for the ideal desired shape of the mirror as well as for other peculiarities of the mirror beamline application. Below, we will validate the point with an example of an elliptically bent mirror.

4. ELLIPTICAL CYLINDER X-RAY MIRROR: BASIC EQUATIONS IN THE TERMS OF THE CONJUGATE PARAMETERS

In this section, we derive basic equations describing the distributions of the tangential surface height, slope, and radius of curvature of an elliptical cylinder x-ray mirror in terms of the mirror beamline application (conjugate) parameters R_1, R_2, and θ_0, where R_1 and R_2 are the respective distances between the first (image) focus F_1 and the second (object) focus F_2, and $\theta_0 \equiv \pi/2 - u$ is the grazing incidence angle at the mirror center – Fig. 2. Many (see, for example, Refs.[9,21-23] and references therein) have previously derived similar equations, but choices made in parameters, definitions and coordinate systems, and in ordering the steps of the derivation can lead to different results.
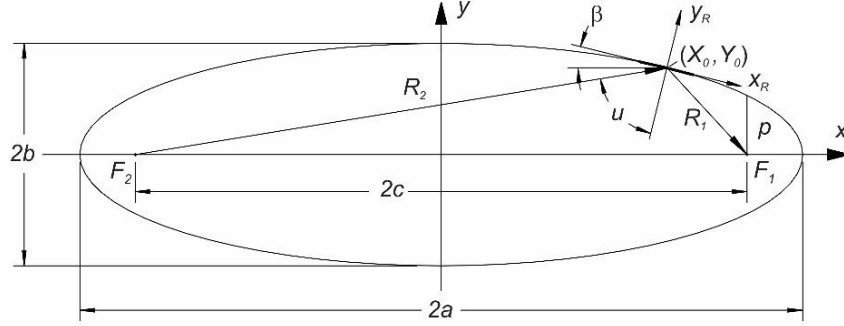

Figure 2. An elliptical cylinder x-ray mirror (bold-line segment) defined with its beamline application (conjugate) parameters R_1, R_2, and $\theta_0 \equiv \pi/2 - u$. F_1 and F_2 are the image and object foci of the mirror. β is the angle between the axis of the ellipse $\vec{x}$ and the tangent of the mirror pole at the canonical Cartesian coordinates (X_0, Y_0). Axes $\vec{x}_R$ and $\vec{y}_R$ define the mirror-related Cartesian coordinate system.

In Fig. 2, the elliptical mirror (bold-line segment) is depicted in the canonical coordinate system, where the mirror center (pole) is shifted from the center of the coordinate system to the point (X_0, Y_0), and the tangent of the pole is tilted by an angle β. This is in contrast to the mirror-related coordinate system $(\vec{x}_R, \vec{y}_R)$ used in ex situ metrology with a surface slope profiler. In these shifted and rotated Cartesian coordinates, the horizontal axis $\vec{x}_R$ is centered in the mirror pole and directed along the pole tangent – Fig. 2. In the course of tuning of bendable mirrors, the measured slope trace has to be compared to the ideal (desired) slope variation also evaluated in the coordinate system of the mirror substrate as measured.

In this section, we present analytical expressions for the height, slope, and radius of curvature distributions of a grazing incidence elliptical cylinder x-ray mirror that are used in our algorithms and dedicated software for optimal tuning of bendable mirrors. The detailed derivations can be found in the report[37] available upon a direct request.

4.1 Relation between the canonical and conjugate parameters of an ellipse

In the canonical form, the shape of the two-dimensional (2D) ellipse in Fig. 2 is determined by the general equation:

$$\frac{x^2}{a^2} + \frac{y^2}{b^2} = 1, \text{ or } y(x) = b\left(1 - \frac{x^2}{a^2}\right)^{1/2}, \tag{35}$$

where a and b are the major and minor semi-axes of the ellipse, respectively. $\vec{x}$ is the horizontal axis of the canonical Cartesian coordinate system, containing the source and focus points; and $\vec{y}$ is the axis orthogonal to $\vec{x}$. We assume that the mirror tangential central line lies in the plane determined with $z = 0$. In an x-ray application of a grazing incidence elliptical mirror, the parameters in Eq. (35) are the real positive numbers that obey a ratio $a \gg b$.

Figure 2 depicts the major parameters of the ellipse used in the derivations below. Basic relations between the canonical and conjugate parameters of an ellipse can be found, for example, in Ref.[38] According to the definition, the ellipse is the locus of points for which the sum of the distances from the two given points (foci) is a constant:

$$a = (R_2 + R_1)/2. \tag{36}$$

In order to derive the relation between the minor semi-axes b and the mirror conjugate parameters,

$$b = \sin\theta_0 (R_1 R_2)^{1/2}. \tag{37}$$

we introduce (36) to the results of Ref.[38] for the radius of curvature Rad in the mirror pole:

$$Rad = \frac{(R_1 R_2)^{3/2}}{ab} = \frac{p}{\sin^3\theta_0}, \tag{38}$$

where $p = b^2/a$ is the semifocal chord (see Fig. 2).

4.2 Spatial and angular position of the pole of an elliptical mirror

To express the position of the mirror pole in the canonical coordinate system as a function of the mirror conjugate parameters, we use the expressions for R_1 and R_2 as the functions of the canonical coordinate x:[38]

$$R_1 = a - eX_0 \text{ and } R_2 = a + eX_0, \tag{39}$$

where e is the eccentricity :

$$e = \frac{c}{a} = \frac{\sqrt{a^2 - b^2}}{a} = \frac{\sqrt{(R_1 + R_2)^2 - 4R_1 R_2 \sin^2\theta_0}}{R_1 + R_2}, \tag{40}$$

where c is a half of the distance between the foci (Fig. 2).

Combining expressions (39) and (40), one can get:

$$X_0 = \frac{(R_2^2 - R_1^2)}{2\sqrt{(R_1 + R_2)^2 - 4R_1 R_2 \sin^2\theta_0}}. \tag{41}$$

An analogous expression for Y_0 is obtained by straightforward algebraic transformations of the canonical equation (35) after substitution of a, b, and X_0 given by Eqs. (36), (37), and (41), respectively:

$$Y_0 = \frac{R_1 R_2 \sin 2\theta_0}{\sqrt{(R_1 + R_2)^2 - 4R_1 R_2 \sin^2\theta_0}}. \tag{42}$$

The expressions (41) and (42) are used below for shifting the coordinate system to the center of the elliptical mirrors. We also need to derive an expression for the angle of rotation β (Fig. 2) of the shifted coordinate system to the mirror-related Cartesian coordinate system defined with axes $\vec{x}_R$ and $\vec{y}_R$.

By differentiation of the known expression[38] for the tangent to the mirror pole in the canonical coordinate system

$$xX_0/a^2 + yY_0/b^2 = 1 \tag{43}$$

and using the expressions above, we get

$$\beta = arc\tan\left[-\frac{b^2}{a^2}\frac{X_0}{Y_0}\right] = -arc\tan\left[\frac{(R_2 - R_1)}{(R_2 + R_1)}\tan\theta_0\right] \text{ or } \cos\beta = \cos\theta_0\frac{R_1 + R_2}{\sqrt{(R_1 + R_2)^2 - 4R_1R_2\sin^2\theta_0}}. \tag{44}$$

4.3 Shape of an elliptical mirror in the mirror-related Cartesian coordinate system as function of the position in the shifted (but not rotated) coordinate system

In the shifted coordinate system, the equation (35) of an ellipse is

$$\frac{(\tilde{x}+X_0)^2}{a^2} + \frac{(\tilde{y}+Y_0)^2}{b^2} = 1, \text{ or } \tilde{y}(\tilde{x}) = b\left(1 - \frac{(\tilde{x}+X_0)^2}{a^2}\right)^{1/2} - Y_0. \tag{45}$$

Next, we apply rotation transformation with angle $-\beta$ [given with Eq. (44)] to $\tilde{y}(x)$ and $\tilde{x}$ coordinates of the ellipse:

$$y_R(\tilde{x}) = \tilde{y}(\tilde{x})\cos\beta - \tilde{x}\sin\beta, \tag{46a}$$

$$x_R(\tilde{x}) = \tilde{x}\cos\beta + \tilde{y}(\tilde{x})\sin\beta. \tag{46b}$$

Technically, the transformations (45) and (46) were performed using analytical capabilities of Mathematica™ software (version 11.1.1). The resultant expressions for the ellipse height distribution $y_R(\tilde{x})$ and tangential positions $x_R(\tilde{x})$ in the rotated coordinate system are

$$y_R(\tilde{x}) = \frac{\sin\theta_0\sqrt{R_1R_2}\sqrt{(R_2 + R_1)^2 - 4(\tilde{x}+X_0)^2} + \tilde{x}(R_2 - R_1)\tan\theta_0 - Y_0(R_2 + R_1)}{\sqrt{(R_2 + R_1)^2 + (R_2 - R_1)^2\tan^2\theta_0}} \tag{47}$$

and

$$x_R(\tilde{x}) = \frac{\tilde{x}(R_2 + R_1)^2 + Y_0\tan\theta_0\left(R_2^2 - R_1^2\right) - \sin\theta_0\tan\theta_0\sqrt{R_1R_2}\left(R_2 - R_1\right)\sqrt{(R_2 + R_1)^2 - 4(\tilde{x}+X_0)^2}}{(R_2 + R_1)\sqrt{(R_2 + R_1)^2 + (R_2 - R_1)^2\tan^2\theta_0}}. \tag{48}$$

The tangential surface slope distribution for the elliptical mirror in the mirror-related coordinate system can be derived by direct differentiation of Eq. (47) and (48):

$$\tan\alpha_R(\tilde{x}) = \frac{dy_R\left(\tilde{x}(x_R)\right)}{dx_R} = \frac{dy_R\left(\tilde{x}\right)}{d\tilde{x}}\cdot\left(\frac{dx_R(\tilde{x})}{d\tilde{x}}\right)^{-1}. \tag{49}$$

This leads to the following expression for the surface slope distribution of an elliptical mirror in the mirror coordinate system

$$\alpha_R(\tilde{x}) = \arctan\left[\frac{-4\sin\theta_0\sqrt{R_1R_2}(R_2 + R_1)(\tilde{x}+X_0) + (R_2^2 - R_1^2)\tan\theta_0\sqrt{(R_2 + R_1)^2 - 4(\tilde{x}+X_0)^2}}{4\sin\theta_0\tan\theta_0\sqrt{R_1R_2}(R_2 - R_1)(\tilde{x}+X_0) + (R_2 + R_1)^2\sqrt{(R_2 + R_1)^2 - 4(\tilde{x}+X_0)^2}}\right]. \tag{50}$$

The expressions for the tangential radius of curvature $Rad_{TAN}(\tilde{x})$ and the grazing incidence angle $\sin\theta(\tilde{x})$ as the functions of the coordinate $\tilde{x}$ are (the corresponding derivations can be found in Ref.[37]):

$$Rad_{TAN}(\tilde{x}) = \frac{\left[(R_2+R_1)^4 - \left(R_2^2 - R_1^2 + 2\tilde{x}\sqrt{(R_1+R_2)^2 - 4R_1R_2\sin^2\theta_0}\right)^2\right]^{3/2}}{4\sqrt{R_1R_2}(R_2+R_1)^4\sin\theta_0} \tag{51}$$

$$\sin\theta(\tilde{x}) = \sin\theta_0\frac{2\sqrt{R_1R_2}\left(R_2+R_1\right)}{\left[(R_2+R_1)^4 - \left(R_2^2 - R_1^2 + 2\tilde{x}\sqrt{(R_1+R_2)^2 - 4R_1R_2\sin^2\theta_0}\right)^2\right]^{1/2}}. \tag{52}$$

4.4 Transition to the positions in the mirror-related Cartesian coordinate

Practically, measurements of the mirror shape are performed in the mirror-related coordinate system (x_R, y_R). Therefore, in order to compare the measured shape with the desired elliptical shape, we need to calculate the surface height distribution $y_R(x_R)$ as a function of x_R, rather than $y_R(\tilde{x})$ as in Eq. (47). The same is true for calculation of the ideal distributions of $\alpha_R(\tilde{x})$, $Rad_{TAN}(\tilde{x})$, and $\sin\theta(\tilde{x})$.

The problem can be solved by reversing Eq. (48) to express the positions $\tilde{x}$ in the shifted (but not rotated) coordinate system as a function $\tilde{x}(x_R)$ of the measured positions x_R in the rotated coordinate system. Then, the calculated positions $\tilde{x}$ are placed into the corresponding expressions (47), (50), (51), and (52) to calculate the corresponding values of the surface height, slope, radius of curvature, and grazing incidence angle. The final set of the analytically calculated ideal distributions (in the height, slope, and curvature domains) are presented as a function of the original positions x_R in the mirror-related coordinate system.

The result of reversing Eq. (48) obtained with Mathematica™ software is as follows:

$$\tilde{x}(x_R) = \frac{\sec\theta_0(R_2+R_1)\sqrt{(R_1+R_2)^2 - 4R_1R_2\sin^2\theta_0}}{(R_2+R_1)^4 + 4R_1R_2(R_2-R_1)^2\sin^2\theta_0\tan^2\theta_0}$$
$$\times\left[x_R(R_2+R_1)^2 - 2\sqrt{R_1R_2}(R_2-R_1)\sin\theta_0\tan\theta_0\left(\sqrt{R_1R_2} - \sqrt{R_1R_2 - x_R^2} - x_R(R_2-R_1)\cos\theta_0\right)\right]. \tag{53}$$

The correctness of the analytical expressions was verified in Ref.[37] by comparing the elliptical mirror profile analytically calculated based on the derived expressions, with the profile numerically generated using the same set of mirror's conjugate parameters. For all the expressions, the difference was on the level of inherent precision of the numerical calculations with IDL™ and OriginPro™ software.

Below, in Sec. 5, we discuss the application of the derived expressions for design and optimal tuning of elliptically bent x-ray mirrors.

5. DESIGN AND OPTIMAL TUNING OF ELLIPTICALLY BENT X-RAY MIRRORS

In this section, we discuss an application of the analytical expressions derived in Sec. 4 for design and optimal tuning of elliptically bent x-ray mirrors. The same approaches can also be applied to the bendable x-ray mirrors with the desired shape different from the elliptical cylinder, if the corresponding expressions are available. Note that similar analytical expressions for hyperbolic cylinder x-ray mirrors have been derived in Ref.[39] available upon direct request.

5.1 Sagittal shaping of substrate for elliptically bent x-ray mirror

In order to precisely specify the optimal sagittal width of substrate for an elliptically bent mirror, we use an analytical expression for the second derivative of the ellipse height variation in the mirror-related coordinate system (see Sec. 2). The expression is derived by differentiating $\tan \alpha_R(\tilde{x})$ given with Eq. (50) in the same manner as Eq. (49):

$$\frac{d^2 y_R\left(\tilde{x}(x_R)\right)}{dx_R^{\,2}} = \frac{d\alpha_R\left(\tilde{x}(x_R)\right)}{dx_R} = \frac{d\alpha_R(\tilde{x})}{d\tilde{x}} \cdot \left(\frac{dx_R(\tilde{x})}{d\tilde{x}}\right)^{-1}. \tag{54}$$

The result of the derivation is (we omit here the sign '-' appeared due to the selected quadrant of the ellipse in Fig. 2):

$$\frac{d^2 y_R(\tilde{x})}{dx_R^{\,2}} = \frac{4(R_2+R_1)^4\left(R_1^2+R_2^2+2R_1R_2\cos 2\theta\right)\sec\theta\sqrt{R_1R_2\left(4R_1R_2+(R_2-R_1)^2\sec^2\theta\right)}\tan\theta}{\left((R_2+R_1)^2\sqrt{(R_2+R_1)^2-4(X_0+\tilde{x})^2}+4(R_2-R_1)\sqrt{R_1R_2}\,(X_0+\tilde{x})\sin[\theta]\tan\theta\right)^3}. \tag{55}$$

In Eq. (3), the variation of the substrate width is defined as a function of the position parameter given in the mirror-related coordinate system. Before substitution to Eq. (3), the second derivative (55) has to be expressed as a function of x_R by using Eq. (53) for $\tilde{x}(x_R)$.

The second derivative (55) and the radius of curvature (51) mutually relate as[38]

$$\left(Rad_{TAN}(\tilde{x})\right)^{-1} \equiv Cur_{TAN}(\tilde{x}) = \frac{d^2 y_R(\tilde{x})}{dx_R^{\,2}} \bigg/ \left(1+\left(\frac{dy_R(\tilde{x})}{dx_R}\right)^2\right)^{3/2} = \frac{d^2 y_R(\tilde{x})}{dx_R^{\,2}} \bigg/ \left(1+\left(\tan\alpha_R(\tilde{x})\right)^2\right)^{3/2}, \tag{56}$$

where $Cur_{TAN}(\tilde{x})$ is the curvature in the elliptical surface. In the case of x-ray mirrors when the surface slope variation is much less than 1, the denominator in Eq. (56) can be approximated with 1. This approximation is often acceptable for evaluating the sagittal width of a substrate for a bendable x-ray mirror [compare with Eq. (3)]:[9,16]

$$w(\tilde{x}) \approx \frac{12}{E\,t_0^3}\left(\frac{C_1+C_2}{2}+\frac{C_1-C_2}{L}\,\tilde{x}\right)Rad_{TAN}(\tilde{x}). \tag{57}$$

In the course of mirror design, the values of the couples C_1 and C_2 are selected by modeling with finite element analysis (FEA) software. The modeling also allows to accounting for the finite thickness of the substrate that, when bending the substrate, leads to a bird-like residual shape in the tangential direction, as well as to an anticlastic deformation in the sagittal directions.[5,6] In order to regain the efficacy of the FEA optimization of the design, one can use the modified method of characteristic functions as suggested and demonstrated in Ref.[11]

5.2 Effect of the finite length of an x-ray mirror used in grazing incidence

The effect of the surface slope error $\Delta(x_i)$ [compare with Eq. (8)] in a particular point x_i (as measured in the mirror related coordinates) of an elliptically bent mirror to the focusing performance of the mirror linearly scales with the distance $r_1(x_i)$ [$r_1(0) \equiv R_1$] from the point to the image focal plane:[10,15]

$$\chi(x_i) = 2r_1(x_i)\tan\Delta(x_i) \approx 2r_1(x_i)\Delta(x_i), \tag{58}$$

where χ_i is the ray position deviation in the focal plane. Equation (58) means that at the same value of slope error, the further the point on the mirror surface from the focal plane, the larger the ray position deviation is. Therefore, the mirror bent to minimize the residual slope variation with respect to the ideal elliptical shape is generally not optimal for focusing the x-rays with the smallest possible width in the focal plane. Optimization of bendable focusing mirrors based

on focusing performance is especially important for beamlines, such as the ALS micro-diffraction beamlines 10.3.2[17] and 12.3.2,[16] where the distance from the mirror to the focal plane is comparable with the mirror length.

Mathematically, optimization of the focusing performance of a bendable mirror consists of minimizing the variance of ray position errors in the focal plane. This is done by applying to $\chi(x_i)$ the linear regression analysis, as discussed in Sec. 3.2, but with the characteristic functions scaled according to Eq. (58):

$$\varepsilon_{\chi i} = \chi(x_i) - \xi_{\chi 0} - \xi_{\chi 1} f_{\chi 1}^*(x_i) - \xi_{\chi 2} f_{\chi 2}^*(x_i), \tag{59}$$

where [compare with Eq. (9)]

$$f_{\chi 1}^*(x_i) = 2r_1(x_i) f_1^*(x_i) \quad \text{and} \quad f_{\chi 2}^*(x_i) = 2r_1(x_i) f_2^*(x_i). \tag{60}$$

At the assumption of a uniformly distributed intensity of the *reflected* x-ray beam, the dispersion functions of the approximation errors $\varepsilon_{\chi i}$ are identical with equal variance σ_χ^2. The rms variation of the resulting (corresponding to the best fit) approximation errors $\varepsilon_{\chi i}^*$ describes the rms width of the focused beam.

Mathematically, the optimization by minimizing the variance of the ray position deviations is equivalent to the surface slope error minimization with the weighted approximation errors scaled as $4r_1^2(x_i)$. Indeed, Eq. (59) can be rewritten in the terms of regression equation (9):

$$v_{\chi i}\varepsilon_i = v_i \Delta(x_i) - v_i \xi_0 - v_i \xi_1 f_1^*(x_i) - v_i \xi_2 f_2^*(x_i). \tag{61}$$

The sum of squared approximation errors in (61), $\sum v_i^2 \varepsilon_i^2$, has the form of Eq. (25) with the weighting parameter

$$\omega_{\chi i} = v_i^2 = 4r_1^2(x_i). \tag{62}$$

5.3 Accounting for the variation of the grazing incidence angle along an elliptically bent x-ray mirror

Let us consider the case of focusing with an elliptically bent mirror of x-ray light beam emitted by a point source with uniform (independent of divergence angle) intensity I_0 – Fig. 3.
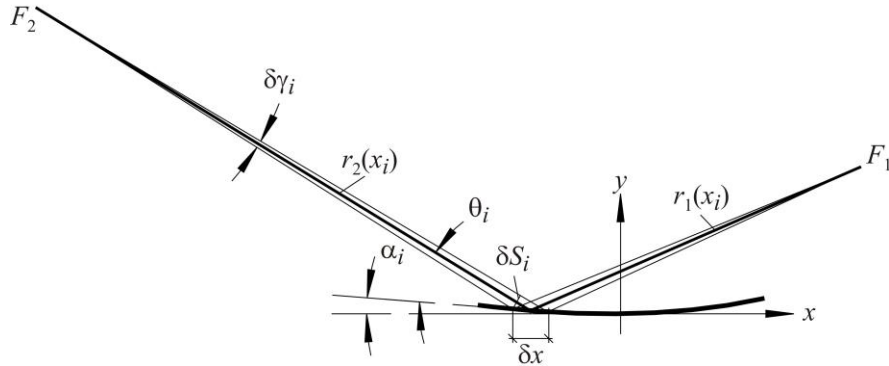

Figure 3. Illustration of the effect of changing the intensity distribution of the reflected light due to the variation of the grazing incidence angle along elliptically bent mirror. The notations are discussed in the text.

In the limit of infinitely small elementary area δx around the tangential position x_i, the light flux $\delta F(x_i)$ incident to the surface area defined by δx depends on the local values of the grazing incidence angle θ_i and the surface slope α_i:

$$\delta F(x_i) = I_0 \cdot \delta\gamma_i = I_0 \cdot \frac{\delta S_i}{r_2(x_i)} = I_0 \cdot \frac{\delta x}{r_2(x_i)} \frac{\sin\theta_i}{\cos\alpha_i} \equiv I_R(x_i) \cdot \delta x. \tag{63}$$

According to Eq. (63), in spite of the uniform distribution of the incident light intensity, the intensity of the reflected light $I_R(x_i)$ is not uniform and depends on the position along the mirror surface.[18] The variation of the reflected intensity $I_R(x_i)$ is accounted in the regression analysis via a corresponding non-normalized weighting parameter:

$$\omega_{\theta i} = \sin \theta_i / \left(r_2(x_i) \cos \alpha_i \right) \tag{64}$$

In order to find an analytical expression for $\sin \theta_i$ for elliptically bent mirrors, we use Eq. (37) for the ellipse minor semi-axis b written for the mirror center and x_i positions:

$$\sin \theta_i = \sin \theta_0 \left(R_1 R_2 \right)^{1/2} / \left(r_1(x_i) r_2(x_i) \right)^{1/2} . \tag{65}$$

In the case of x-ray grazing incidence mirrors under consideration, the surface slope variation is usually less than ± 10 mrad. Correspondingly, the variation of $\cos \alpha_i$ is less than 10^{-4} and can be ignored in the denominator of Eq. (64). Introducing (65) to (64), we get

$$\omega_{\theta i} = \sin \theta_0 \left(R_1 R_2 \right)^{1/2} / \left(r_1^{1/2}(x_i) r_2^{3/2}(x_i) \right), \tag{66}$$

5.4 Non-uniform distribution of intensity of the incident x-ray beam

So far, we were assuming that the incident x-ray beam has a uniform intensity distribution. In the frame of the approach developed above in this section, accounting for non-uniform distribution of the incident x-ray beam intensity is rather straightforward if one defines the distribution as a function of the position along the mirror x_i,

$$I_{In} = I_0 \cdot \varphi(x_i) . \tag{67}$$

The intensity distribution function $\varphi(x_i)$ has to be included into the non-normalized weighting parameter $\omega_{\theta i}$ describing the effect of variation of the grazing incidence angle with Eq. (66):

$$\omega_{\theta i} = \varphi(x_i) \sin \theta_0 \left(R_1 R_2 \right)^{1/2} / \left(r_1^{1/2}(x_i) r_2^{3/2}(x_i) \right). \tag{68}$$

A more natural definition of the intensity distribution would be in the angular terms:

$$I_{In} = I_0 \cdot \varphi(\gamma) , \tag{69}$$

where $\gamma(x_i) \equiv \gamma_i$ is the angle determining the direction of the light ray incident to the mirror surface point with the tangential coordinate x_i – Fig. 4.
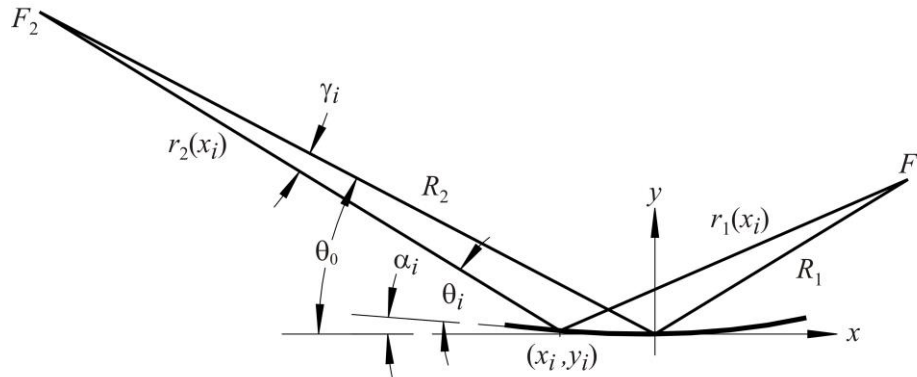

Figure 4. Reflection from an elliptically bent mirror of a beam with intensity distribution depending on the angle γ_i counted with respect to the direction to the center of the mirror where $\gamma = 0$. Other notations are defined in the text.

Without losing the generality of the consideration, the angle γ_i is counted with respect to the direction to the center of the mirror, where $\gamma = 0$. We also assume that at $x_i < 0$, the angles α_i and γ_i are negative, $\alpha_i < 0$ and $\gamma_i < 0$.

From Fig. 4, it is evident that

$$\gamma_i = \theta_0 - \theta_i + \alpha_i \tag{70}$$

Because all angles in Eq. (70) have comparable values, for calculation of γ_i corresponding to the position x_i in the mirror-related coordinates, one has to use the exact expressions for the local grazing incidence angles given with Eqs. (50), (52), and (53).

5.5 Weighting parameter associated with the geometrical peculiarities of an elliptically bent x-ray mirror

The product of Eqs. (62) and (68) describes the weighting parameter associated with the geometrical peculiarities of an x-ray mirror used in grazing incidence arrangement:

$$\omega_{Mi} = \varphi(x_i) \cdot r_1^{3/2}(x_i) \cdot r_2^{-3/2}(x_i), \tag{71}$$

where the constant terms in (62) and (68) are omitted because the scaling factors do not affect the result of application of the regression analysis, as discussed in Sec. 3.3.

Let us now derive analytical expressions for $r_1(x_i)$ and $r_2(x_i)$ for the case of an elliptically bent mirror. For high quality x-ray optics, one can use the expressions, corresponding to an ideally shaped mirror (no surface errors). Using the relations (39), written for the position $\tilde{x}_i + X_0$ in the shifted coordinate system, and Eqs. (40) and (41), one can derive dependencies of the focal distances on the position $\tilde{x}_i$:

$$r_1(\tilde{x}_i) = R_1 - \tilde{x}_i \cdot e = R_1 - \tilde{x}_i \cdot \frac{\sqrt{(R_1 + R_2)^2 - 4R_1 R_2 \sin^2 \theta_0}}{R_1 + R_2} \quad \text{and} \tag{72b}$$

$$r_2(\tilde{x}_i) = R_2 + \tilde{x}_i \cdot e = R_2 + \tilde{x}_i \cdot \frac{\sqrt{(R_1 + R_2)^2 - 4R_1 R_2 \sin^2 \theta_0}}{R_1 + R_2}. \tag{72b}$$

The exact relation between the given $\tilde{x}_i$ in Eqs. (72) and the corresponding position x_i in the mirror based coordinate system, which corresponds to the same distances between a particular point on the ellipse curve in Fig. 2 and the image and object foci F_1 and F_1 (Fig. 3), is rather unwieldy. Much simpler expressions are obtained with an approximation $\tilde{x}_i \approx x_i \cos \beta$ that provides reasonable accuracy for accounting of the mirror geometry effects in the shape optimization of a bendable elliptical mirror. In this case, by using Eq. (44) one gets:[10,15]

$$r_1(x_i) \approx R_1 - x_i \cdot \cos \theta_0 \quad \text{and} \quad r_2(x_i) \approx R_2 + x_i \cdot \cos \theta_0. \tag{73}$$

Substitution of (73) to (71) gives a relatively simple, but sufficiently accurate, scaling of the weighting parameter as a function of the tangential position in the mirror based coordinate system:

$$\omega_{Mi} \approx \varphi(x_i) \cdot (R_1 - x_i \cdot \cos \theta_0)^{3/2} \cdot (R_2 + x_i \cdot \cos \theta_0)^{-3/2}. \tag{74}$$

The weighting parameter given by Eq. (74) is not normalized to obey the condition $\sum \omega_{Mi} = n$ that, in principle, does not affect the result of the linear regression analysis, described in Sec. 3.3. However, if the weighting parameter is normalized to its average value $\bar{\omega}_M = n^{-1} \sum \omega_{Mi}$,

$$\omega_{Mi}^* = \omega_{Mi} / \bar{\omega}_M, \tag{75}$$

the resulting (corresponding to the best fit) rms variation of the approximation error can be thought of as an estimation of the *effective* residual slope error (rms) of the elliptically bent mirror with optimized focusing performance.

6. APPLICATION OF THE DEVELOPED ALGORITHMS AND SOFTWARE TO OPTIMAL TUNING OF AN ELLIPTICALLY BENT X-RAY MIRROR

In this section, we apply the developed analytical methods and dedicated bending optimization software to a bendable elliptically cylindrical mirror M4 for the ALS beamline (BL) 10.3.2.

ALS BL 10.3.2 is a versatile environmental and materials science tool, primarily designed for heavy metal speciation and location. The x-ray beam is focused via a KB mirror system to the sample location with a spot size of about 1 µm. A full description of this beamline and its capabilities, as of 2004, can be found in Ref.[40] The BL end-station optical schematic includes three bendable mirrors. A vertically deflecting parabolic mirror (M2) collimates the beam to a two-crystal monochromator. A second parabolic cylinder mirror (M3) focuses the beam vertically, and an elliptical mirror (M4) focuses the beam horizontally. The performance of the beamline, namely the spatial and energy resolutions of the measurements, depends significantly on the collimation properties of M2 mirror and focusing properties of the mirrors M3 and M4.

Mirrors M2, M3 and M4 are all bendable mirrors, based on a similar design approach,[14] each with two bending, cantilever-like, couples attached to ends of the mirror substrate (Fig. 5). In this design, the measure of the applied bending couples is the value of the linear translation (in microns) of a Pico-motor that stresses the corresponding cantilever spring.
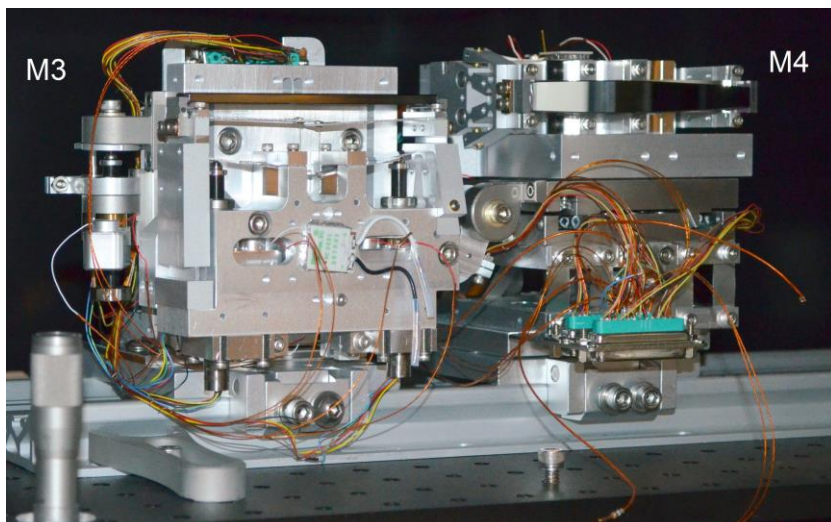

Figure 5: The ALS BL 10.3.2 mirrors M3 and M4 prepared for surface slope measurements with the XROL DLTP.[23,24] The high temperature stability of the mirrors is due to the active temperature stabilization with Peltier elements. One of them is seem as attached to the body of M3 mirror.

6.1 Characteristic functions of the ALS BL 10.3.2 M2 mirror benders

We selected the M4 mirror to illustrate the developed bending optimization methods because the mirror clear aperture length of 80 mm is comparable with the mirror image focus of about 120 mm. The overall size of the mirror substrate is 102 mm (length) × 13 mm (width at middle), with a strong variation of the sagittal width of the substrate. This arrangement allows us to test the sensitivity of the shape optimization to the weighting functions dependent on the mirror geometry (see Sec. 5).

The beamline arrangement of the mirror is specified with the conjugate parameters of a source distance R_2, fixed grazing incidence angle θ_0, and focal (image) distance R_1:

$$R_2 = 2218.3\,\text{mm}, \quad \theta_0 = 4.0\,\text{mrad, and } R_1 = 118.9\,\text{mm}. \tag{76}$$

With the conjugate parameters (76), the mirror radius of curvature varies from approximately 80 m down to about 30 m.

The surface slope measurements with the mirror were performed with the developmental long trace profiler[23,24] available at the ALS X-Ray Optics Lab. The mirror tuning was performed after installation of a new substrate and approximate shaping using a Fizeau interferometer.

First, the characteristic functions of the mirror's upstream $f_1^*(x_i)$ and downstream $f_2^*(x_i)$ benders were constructed (Fig. 6) based on three surface slope measurements, as described in Sec. 31 with Eq. (7), with the changes of the bending couples, δC_1 and δC_2 of 50 µm. Note that the evaluation of a characteristic function from the difference of two surface slope measurements has a differential nature. Therefore, the systematic errors common for the measurements do not affect the result.
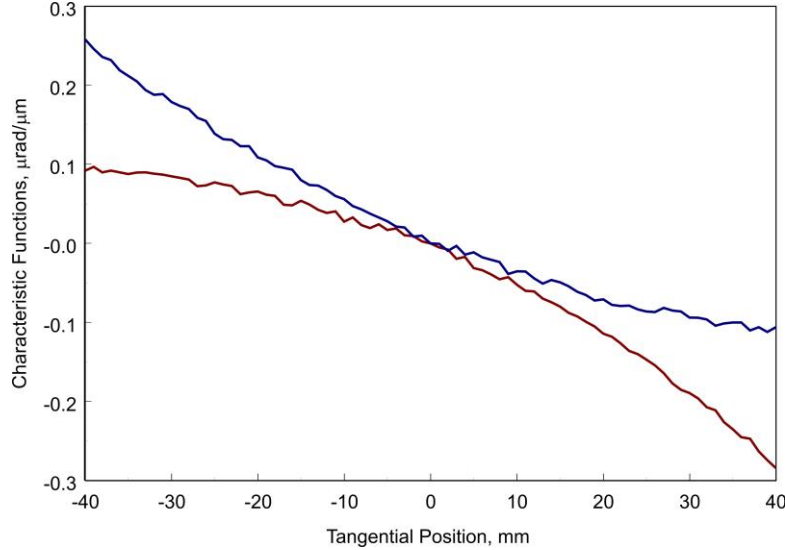
Figure 6: The upstream (the upper, blue line) and the downstream (the lower, red line) characteristic functions of M4 mirror's benders evaluated from three DLTP measurements performed at the bending couples sequentially changed by 50 µm. As expected, the upstream (downstream) characteristic function is steeper at the upstream (downstream) part of the mirror reflecting the stronger effect to this part by the corresponding bending couple.

6.2 Optimization software

At the ALS XROL, we have realized the tuning algorithms discussed in detail throughout this paper in dedicated software developed in the IDL development environment platform. The software allows optimization of the shape of elliptical or parabolic bendable mirrors using the analytical equations in Secs. 4 and 5 to calculate the ideal mirror shape and the weighting functions.

The software predicts the best-fit adjustments to the bender's couples measured in the same units as the changes to the couples applied for measurement of the characteristic functions. The adjustment are given with respect to the bender settings of one of the three measurements, as well as with respect to an additional, fourth measurement that can be carried out to test the result of the first iteration. The software also estimates the prediction errors for the regressed parameters.

An additional iteration, if needed, uses the same data for calculation of the characteristic function. Therefore, additional iteration generally requires only one additional measurement. Practically, in order to optimally set the benders of a properly designed elliptical or parabolic mirror, we usually need 1 or 2 iterations.

6.3 Optimal tuning of the bendable elliptically cylinder M4 mirror for the ALS BL 10.3.2

The contribution of different weighting factors to the mirror M4 shape optimization is illustrated in a series of tunings performed with the same measured slope traces, but when fitting with different weighting functions.

Figure 7 shows the residual [after subtraction of the ideal ellipse given by the conjugate parameters (76)], slope trace of the clear aperture of the M4 mirror before the bender's optimization. The peak-to-valley (PV) surface slope variation is about 23 µrad.
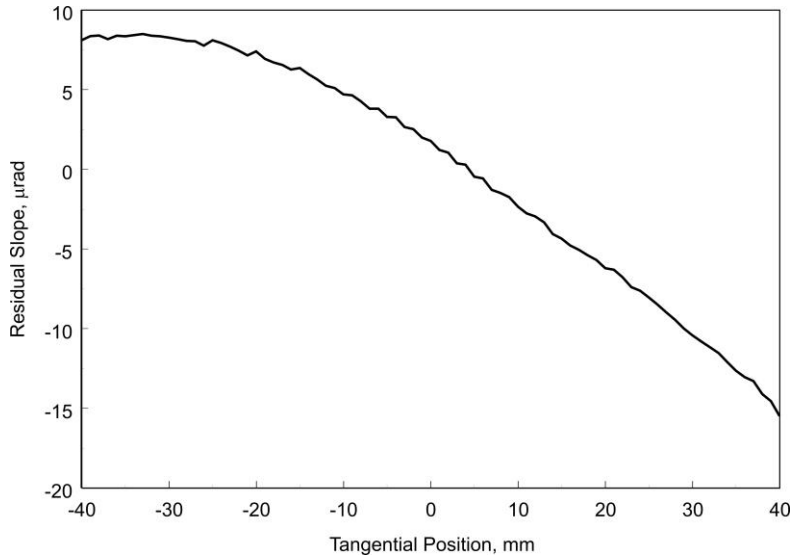

Figure 7: Residual slope, after subtraction of the ideal ellipse, of the central tangential trace along the clear aperture of the M4 mirror before the bender's optimization. The peak-to-valley surface slope variation is about 23 µrad.

The residual slope trace of the clear aperture of the M4 mirror after applying to the bender's couples the adjustments predicted without accounting for the peculiarities of the mirror geometry and beamline application, as well as the x-ray beam intensity variation (see Sec. 5) is presented in Fig. 8. The third order trend in the residual slope trace is very characteristic of bendable mirror (see discussion in Sec. 5.1). It corresponds to a 4th order "bird-like" shape in the height domain. The rms and PV variations of the residual slope are 0.574 µrad and 2.3 µrad, respectively.
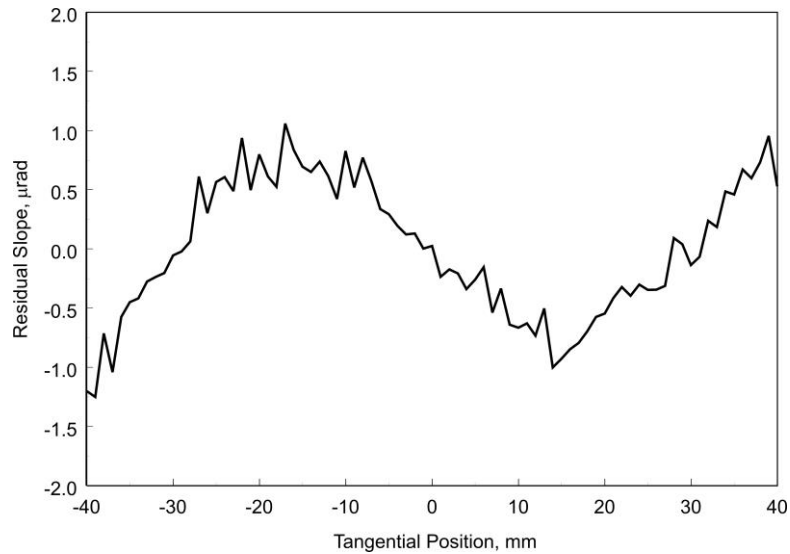

Figure 8: Residual slope, after subtraction of the ideal ellipse, of the central tangential trace along the clear aperture of the M4 mirror after adjusting the couples to the optimal settings predicted without accounting for the peculiarities of the mirror geometry and beamline application, as well as the x-ray beam intensity variation. The rms and PV variations of the residual slope are 0.574 µrad and 2.3 µrad, respectively.

Accounting for the weighting factors reflecting the mirror geometry (see Secs. 5.2 and 5.3), but still with uniform illumination, leads to a noticeable, ~ 0.7 µrad (PV), change of the residual slope variation depicted in Fig. 9.
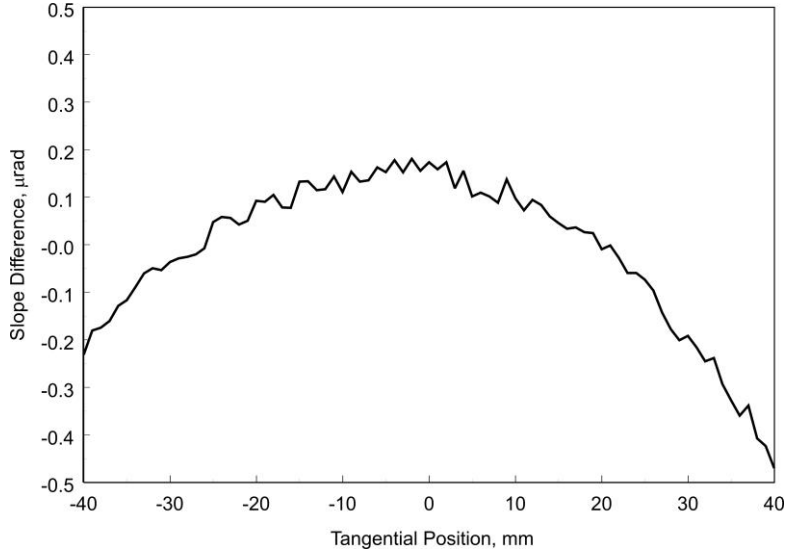

Figure 9: Difference of the residual slope traces corresponding to the adjustments of the bending couples without and with accounting for the peculiarities of the mirror geometry and beamline application. The both tuning options assume uniform x-ray beam intensity distribution along the mirror. The PV change of the mirror surface slope is about 0.7 µrad.

Let us now allow for a non-uniform distribution of the x-ray beam intensity, described by the Gaussian distribution

$$I(x_i) = I_0 \cdot e^{-x_i^2/(2\sigma^2)} \tag{77}$$

with a standard deviation of $\sigma = 10$ mm that corresponds to a full-width-half-maximum of the beam footprint on the mirror surface of approximately 23 mm. Figure 10 shows the residual slope trace after applying adjustments to the bender's couples predicted accounting for the peculiarities of the mirror geometry the non-uniformity of x-ray beam intensity distribution (77).
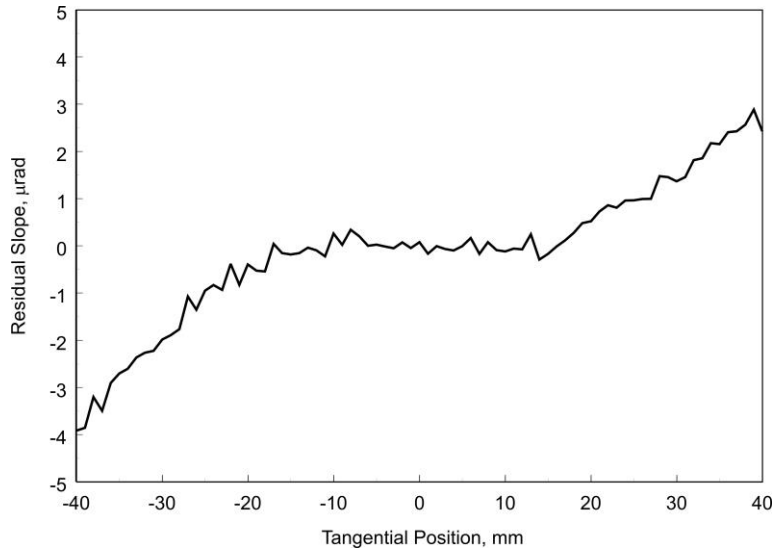

Figure 10: Residual slope, after subtraction of the ideal ellipse, of the central tangential trace along the clear aperture of the M4 mirror after adjusting the couples to the optimal settings predicted with accounting for the peculiarities of the mirror geometry, beamline application, and the non-uniformity of the x-ray beam intensity distribution given with Eq. (77). The rms and PV variations of the residual slope are 1.46 µrad and ~ 6.5 µrad, respectively.

Table 1 summarizes the couples' adjustments and their standard deviations predicted with the developed software for the three cases considered above: (i) without weighting function (Fig. 8), (ii) with waiting function accounting for the mirror geometry (Fig. 9), and (iii) with accounting for the non-uniform distribution of the x-ray beam intensity (Fig. 10). From Table 1, it is evident that a relatively small mistuning of the BL 10.3.2 mirror M4 benders can dramatically change the beamline performance of the mirror.

Table 1. The BL 10.3.2 mirror M4 couples' adjustments and their standard deviations predicted with the developed software for the three case considered above: (i) without weighting function, (ii) with waiting function accounting for the mirror geometry, and (iii) with accounting for the non-uniform distribution of the x-ray beam intensity.

Tuning options	ΔC_1 (upstream), µm	σ_{C_1}, µm	ΔC_1 (downstream), µm	σ_{C_2}, µm
(i)	-59.7	1.8	-8.4	1.9
(ii)	-62.9	2.3	-5.7	1.9
(iii)	-62.5	2.6	-18.1	2.4

Additional accounting for the non-uniform distribution of the x-ray beam intensity dramatically changes the residual slope variation. The optimization decreases the slope error over the mostly illuminated central part of the mirror, shifting the slope variation to the edges of the clear aperture. In spite of the ~2.5 fold increase of the rms slope variation compared to Fig. 8, the beamline performance of the mirror illuminated with the non-uniform intensity will be significantly better. This can be characterized with the value of the effective (weighted rms) residual slope variation equal to the square-root of the sum in Eq. (25) divided by the number of points in the trace. The resulted weighted rms residual slope variations for the cases in Figs. 9 and 10 are 0.567 µrad and 0.143 µrad, respectively. As expected, with a narrower beam intensity distribution, the effective rms slope variation is much smaller, by a factor of about 4.

7. CONCLUSIONS

We have systematically discussed the experimental, analytical, and numerical methods developed at the ALS X-Ray Optics Lab for ex situ (at optics lab) calibration and precision shaping of bendable x-ray mirrors. We concentrate the discussion on the methods that are based on geometrical optics and optical surface slope metrology available at the ALS XROL with three state-of-the-art surface slope profilers, LTP-II, DLTP, and OSMS.

The developed methods and dedicated software allow optimization of the beamline performance of bendable mirrors not only by adjustment of the mirror shape to minimize the root-mean-square variation of residual (after subtraction of the ideal desired shape) slope deviations from ideal (specified) surface figure, but also by optimization with accounting for the peculiarities of the mirror geometry and beamline application. In this case, the figure of merit for the tuning is the minimum of the rms size of the focused beam. Note that the discussed methods help getting the surface profile as close to the desired shape as possible, partially compensating for the design and fabrication errors.

The efficacy of the optimization is demonstrated with examples of optimal tuning of the elliptically bendable cylindrical mirror M4 designed for the ALS beamline 10.3.2.

We should also mention that the same mathematical approach can be used for additional optimization of the beamline performance of the bendable mirror by optimization of the conjugate parameters of the at-beamline optical application, after the best tuning of the bending couples is completed. This possibility has been discussed in detail in Ref.[41]

In Ref.,[11] evaluation of characteristic functions based on Finite Element Analysis of a complete bendable mirror assembly has been suggested and investigated. Calculating FEA-based characteristic functions and applying the regression analysis methods discussed in the present work in the design stage would allow better understanding of the design of the bender's adjustment mechanism and permit that design to be better matched to the required beamline performance of the mirror.

The presented analytical foundations are generally applicable to in situ optimization of bendable optics as the ones developed at the ALS XROL,[27-29] as well as to the extension of the ex situ optimization to account for diffraction effects.[18]

ACKNOWLEDGEMENTS

Disclaimer

REFERENCES

[1] Kirkpatrick, P. and Baez, A. V., "Formation of Optical Images by X-Rays," J. Opt. Soc. Am. 38, 766 (1948); https://doi.org/10.1364/JOSA.38.000766.

[2] Wolter, H., "Glancing Incidence Mirror Systems as Imaging Optics for X-rays," Annalen der Physik. 6th Ser. 10, 94 (1952); doi:10.1002/andp.19524450108.

[3] Wolter, H., "A Generalized Schwarzschild Mirror System For Use at Glancing Incidence for X-ray Imaging," Annalen der Physik. 6th Ser. 10, 286 (1952); doi:10.1002/andp.19524450410.

[4] Kelez, N., Bozek, J., Chuang, Y.-D., Duarte, R., Lee, D. E., McKinney, W., Yashchuk, V., and Yuan, S., "Design, Modeling, and Optimization of Precision Bent Refocus Optics - LCLS AMO KB Mirror Assembly," Proc. of FEL2009, 546-549 (Liverpool, UK, 2009); http://accelconf.web.cern.ch/accelconf/FEL2009/papers/wepc20.pdf.

[5] Howells, M. R. and Lunt, D., "Design considerations for adjustable-curvature, high-power, X-ray mirrors based on elastic bending," Opt. Eng. 32(8), 1981-1989 (1993).

[6] Howells, M. R., Cambie, D., Duarte, R. M., Irick, S., MacDowell, A. A., Padmore, H. A., Renner, T. R., Rah, S. Y., and Sandler, R., "Theory and practice of elliptically bent x-ray mirrors," Opt. Eng., 39(10), 2748-2762 (2000); https://doi.org/10.1117/1.1289879.

[7] McKinney, W. R., Irick, S. C., Kirschman, J. L., MacDowell, A. A., Warwick, A., and Yashchuk, V. V., "New Procedure for the Adjustment of Elliptically Bent Mirrors with the Long Trace profiler," Proc. SPIE 6704, 67040G (2007); doi: 10.1117/12.736860.

[8] McKinney, W. R., Kirschman, J. L., MacDowell, A. A., Warwick, T., Yashchuk, V. V., "Optimal tuning and calibration of bendable mirrors with slope measuring profilers," Opt. Eng. 48(8), 083601-1-8 (2009); doi:10.1117/1.3204235.

[9] McKinney, W. R., Yashchuk, V. V., Goldberg, K. A., Howells, M., Artemiev, N. A., Merthe, D. J., and Yuan, S., "Design optimization of bendable x-ray mirrors," Proc. SPIE 8141, 81410K-1-14 (2011); doi: 10.1117/12.894175.

[10] McKinney, W. R., Yashchuk, V. V., Merthe, D. J., Artemiev, N. A., and Goldberg, K. A., "Ex situ tuning of bendable x-ray mirrors for optimal beamline performance," Proc. SPIE 8501, 850109-1-8 (2012).

[11] Artemiev, N. A., Chow, K. P., La Civita, D., Merthe, D. J., Chuang, Y.-D., McKinney, W. R., and Yashchuk, V. V., "Optimal setting of bendable optics based on FEA calculations," Proc. SPIE 8501, 850107-1-18 (2012).

[12] Artemiev, N. A., Chow, K. P., Merthe, D. J., Rotenberg, E., Takakuwa, J. H., Warwick, T., and Yashchuk, V. V., "Two-foci, bendable mirrors for the ALS MAESTRO beamline: design and metrology characterization and optimal tuning of the mirror benders," Proc. SPIE 8848, 88480D-1-14 (2013); doi: 10.1117/12.2024675.

[13] Artemiev, N. A., Smith, B. V., Domning, E. E., Lacey, I., and Yashchuk, V. V., "Angular calibration of surface slope measuring profilers with a bendable mirror," Proc. SPIE 9206, 92060G/1-14 (2014) [doi: 10.1117/12.2061948].

[14] Yuan, S., Church, M., Yashchuk, V. V., Goldberg, K. A., Celestre, R., McKinney, W. R., Kirschman, J., Morrison, G., Null, T., Warwick, T., and Padmore, H. A., "Elliptically Bent X-ray Mirrors with Active Temperature Stabilization," X-Ray Optics and Instrumentation 2010, 784732/1-9 (2010).

[15] Yashchuk, V. V., Merthe, D. J., Goldberg, K. A., Artemiev, N. A., Celestre, R., Domning, E. E., Kunz, M., McKinney, W. R., Morrison, G. Y., Smith, B. V., Tamura, N., "Experimental methods for optimal tuning and alignment of bendable mirrors for diffraction-limited soft x-ray focusing," Journal of Physics: Conf. Ser. 425, 152003 (2013); http://iopscience.iop.org/1742-6596/425/15/152003.

[16] Yashchuk, V. V., Morrison, G. Y., Church, M., Artemiev, N. A., Celestre, R., Domning, E. E., Howells, M., Kunz, M, McKinney, W. R., Merthe, D. J., Smith, B. V., Tamura, N., and Padmore, H. A., "Bendable Kirkpatrick-Baez mirrors for the ALS micro-diffraction beamline 12.3.2: design, metrology, and performance," Journal of Physics: Conf. Ser. 425, 152004 (2013); http://iopscience.iop.org/1742-6596/425/15/152004.

[17] Yashchuk, V. V., Morrison, G. Y., Marcus, M. A., Domning, E., Merthe, D. J., Salmassi, F., and Smith, B., "Performance Optimization of a Bendable Parabolic Collimating X-Ray Mirror for the ALS Micro-XAS Beamline 10.3.2," J. Synch. Rad. 22(3), 666-674 (2015); doi:10.1107/S1600577515001459.

[18] Goldberg K. A. and Yashchuk, V. V., "Optimized mirror shape tuning using beam weightings based on distance, angle of incidence, reflectivity, and power," Rev. Sci. Instrum. 87(5), 051805 (2016); doi: 10.1063/1.4950747.

[19] Yashchuk, V. V., Artemiev, N. A., Lacey, I., McKinney, W. R., and Padmore, H. A., "A new X-ray optics laboratory (XROL) at the ALS: Mission, arrangement, metrology capabilities, performance, and future plans," Proc. SPIE 9206, 92060I/1-19 (2014); doi:10.1117/12.2062042.

[20] Yashchuk, V. V., Artemiev, N. A., Lacey, I., McKinney, W. R., and Padmore, H. A., "Advanced environmental control as a key component in the development of ultra-high accuracy ex situ metrology for x-ray optics," Opt. Eng. 54(10), 104104/1-14 (2015); doi: 10.1117/1.OE.54.10.104104.

[21] Kirschman, J. L., Domning, E. E., McKinney, W. R., Morrison, G. Y., Smith, B. V., and Yashchuk, V. V., "Performance of the upgraded LTP-II at the ALS Optical Metrology Laboratory," Proc. SPIE 7077, 70770A/1-12 (2008); doi: 10.1117/12.796335 1

[22] Nikitin, S. M., Gevorkyan, G. S., McKinney, W. R., Lacey, I., Takacs, P. Z., and Yashchuk, V. V., "New twist in the optical schematic of surface slope measuring long trace profiler," Proc. SPIE 10388, 103850I-1-17 (2017); doi: 10.1117/12.2274400.

[23] Barber, S. K., Morrison, G. Y., Yashchuk, V. V., Gubarev, M. V., Geckeler, R. D., Buchheim, J., Siewert, F., and Zeschke, T., "Developmental long trace profiler using optimally aligned mirror based pentaprism," Opt. Eng. 50(5), 053601-1-10 (2011); ttps://doi.org/10.1117/1.3572113.

[24] Lacey, I., Artemiev, N. A., Domning, E. E., McKinney, W. R., Morrison, G. Y., Morton, S. A., Smith, B. V., and Yashchuk, V. V., "The developmental long trace profiler (DLTP) optimized for metrology of side-facing optics at the ALS," Proc. SPIE 9206, 920603/1-11 (2014); doi:10.1117/12.2061969.

[25] Lacey, I., Adam, J., Centers, G., Gevorkyan, G. S., Nikitin, S. M., Smith, B. V., and Yashchuk, V. V., "Development of a high performance surface slope measuring system for two-dimensional mapping of x-ray optics," Proc. SPIE 10385, 103850G-1-13 (2017); doi: 10.1117/12.2273029.

[26] Yashchuk, V. V., Centers, G., Gevorkyan, G. S., Lacey, I., and Smith, B. V., "Correlation methods in optical metrology with state-of-the-art x-ray mirrors," Proc. SPIE 10612, 106120O/1-23 (2018); doi: 10.1117/12.2305441.

[27] Merthe, D. J., Yashchuk, V. V., Goldberg, K. A., Kunz, M., Tamura, N., McKinney, W. R., Celestre, R. S., Morrison, G. Y., Anderson, E., Smith, B. V., Domning, E. E., and Padmore, H. A., "Methodology for Optimal In Situ Alignment and Setting of Bendable Optics for Diffraction-Limited Focusing of Soft X-Rays," Proc. SPIE 8501, 850108-1-16 (2012); doi: 10.1117/12.930023.

[28] Merthe, D. J., Yashchuk, V. V., Goldberg, K. A., Kunz, M., Tamura, N., McKinney, Artemiev, N. A., Celestre, R. S., Morrison, G. Y., Anderson, E., Smith, B. V., Domning, E. E., Rakawa, S. B., and Padmore, H. A., "Methodology for optimal in situ alignment and setting of bendable optics for nearly diffraction-limited focusing of soft x-rays," Opt. Eng. 52(3), 033603-1-13 (2013); http://dx.doi.org/10.1117/1.OE.52.3.033603.

[29] Merthe, D. J., Goldberg, K. A., Yashchuk, V. V., McKinney, W. R., Celestre, R., Mochi, I., MacDougall, J., Morrison, G. Y., Rakawa, S. B., Anderson, E., Smith, B. V., Domning, E. E., and Padmore, H., "In situ fine tuning of bendable soft x-ray mirrors using a lateral shearing interferometer," Nucl. Instr. and Meth. A 710, 82-86 (2013); http://dx.doi.org/10.1016/j.nima.2012.10.105.

[30] Hignette, O., Freund, A., and Chinchio, E., "Incoherent X-ray mirror surface metrology," Proc. SPIE 3152, 188-199 (1997); doi: 10.1117/12.295559.

[31] Roark, R. J., [Formulas for Stress and Strain], McGraw-Hill, New York (1964).

[32] Hudson, D. J., [Statistics: Lectures on Elementary Statistics and Probability], Geneva (1964); In Russian: Hudson, D. J., [Statistics for Physicists], Moscow, Mir (1970).

[33] Yashchuk, V. V., "Positioning errors of pencil-beam interferometers for long-trace profilers," Proc. SPIE 6317, 6317 0A-1-12 (2006); doi: 10.1117/12.677956.

[34] Plackett, R. L., [Principles of Regression Analysis], Oxford, At The Clarendon Press (1960).

[35] Neter, J. and Wasserman, W., [Applied Linear Statistical Models], London, Inwin-Dorsey International (1974).

[36] Kendall, M. and Stuart, A., [The Advance theory of Statistics], vol.2, New York, Oxford University Press (1979).

[37] Yashchuk, V. V., Lacey, I., McKinney, W.R., Nikitin, S. M., and Warwick, T., "Elliptical cylinder x-ray mirror: Basic equations in the terms of the conjugate parameters," Light Source Beam Line Note LSBL-1346 (ALS, Berkeley, March 12, 2018).

[38] Bronshtein, I. N., Semendyayev, K. A., Musiol, G., and Muehling, H., [Handbook of Mathematics,] 5th Ed., Springer, Berlin (2007), pp. 198-200.

[39] Yashchuk, V. V., Nikitin, S. M., Lacey, I., and McKinney, W. R., "Hyperbolic cylinder x-ray mirror: Basic equations in the terms of the conjugate parameters," Light Source Beam Line Note LSBL-1320 (ALS, Berkeley, June 20, 2017).

[40] Marcus, M. A., MacDowell, A. A., Celestre, R., Manceau, A., Miller, T., Padmore, H. A. and Sublett, R. E., "Beamline 10.3.2 at ALS: a hard X-ray microprobe for environmental and materials sciences," J. Synch. Rad. 11, 239–247 (2004); https://doi.org/10.1107/S0909049504005837.

[41] Yashchuk, V. V., Lacey, I., Gevorkyan, G., McKinney, W., Nikitin, S., Smith, B., and Warwick, T., "Ex situ metrology of aspherical pre-shaped x-ray mirrors at the Advanced Light Source," Abstract of an invited talk at the 6th International Workshop on X-ray Optics and Metrology, The SRI2018 Satellite Workshop (IWXM 2018) (Hsinchu, Taiwan, June 6-9, 2018); the corresponding proceeding manuscript is in preparation.